This is the accepted version of the manuscript published on Small. The article can be found under https://doi.org/10.102/smll.201804557

Single Domain 10 nm Ferromagnetism Imprinted on Superparamagnetic Nanoparticles Using Chiral Molecules

Guy Koplovitz, Gregory Leitus, Supriya Ghosh, Brian P. Bloom, Shira Yochelis, Dvir Rotem, Fabio Vischio, Marinella Striccoli, Elisabetta Fanizza, Ron Naaman, David H. Waldeck, Danny Porath, and Yossi Paltiel**

The rapid growth in demand for data and the emerging applications of Big Data require the increase of memory capacity. Magnetic memory devices are among the leading technologies for meeting this demand; however, they rely on the use of ferromagnets that creates size reduction limitations and poses complex materials requirements. Usually magnetic memory sizes
are limited to 30–50 nm. Reducing the size even further, to the ≈10–20 nm scale, destabilizes the magnetization and its magnetic orientation becomes susceptible to thermal fluctuations and stray magnetic fields. In the present work, it is shown that 10 nm single domain ferromagnetism can be achieved. Using asymmetric adsorption of chiral molecules, superparamagnetic iron oxide nanoparticles become ferromagnetic with an average coercive field of ≈80 Oe. The asymmetric adsorption of molecules stabilizes the magnetization direction at room temperature and the orientation is found to depend on the handedness of the chiral molecules. These studies point to a novel method for the miniaturization of ferromagnets (down to ≈10 nm) using established synthetic protocols.

The rapid growth in demand for data (such as videos, pictures, and audio) and the emerging applications of Big Data require the increase of memory capacity, as well as faster and more energy efficient nonvolatile memory devices. Spintronic-based magnetic memory devices are among the leading technologies for meeting this demand.[1–4] Spintronics technology is already industrialized and widely used in devices such as hard disk drives and magnetic random access memory.[4,5] All spintronic devices require the use of mag-netic materials as the memory storage medium and for generating spin polarized currents. The use of ferromagnets (FMs) for producing the spin current creates size reduction limitations and poses complex materials requirements.[3–5]

The size reduction limitation arises from the physicochemical nature of the materials, specifically FMs, whose mag-netic properties are comprised from their magnetic domains at smaller sizes.[6] Typically, magnetic domains in a ferro-magnet are micrometer in size, so that reducing the size to ≈50 nm scale cre-ates a single magnetic domain with high coercivity.

The exact location of the transition from multiple domain to single domain of Fe3O4 depends on both size and shape. For example, in cuboidal particles the critical diameter for forming a multidomain structure has been theoretically

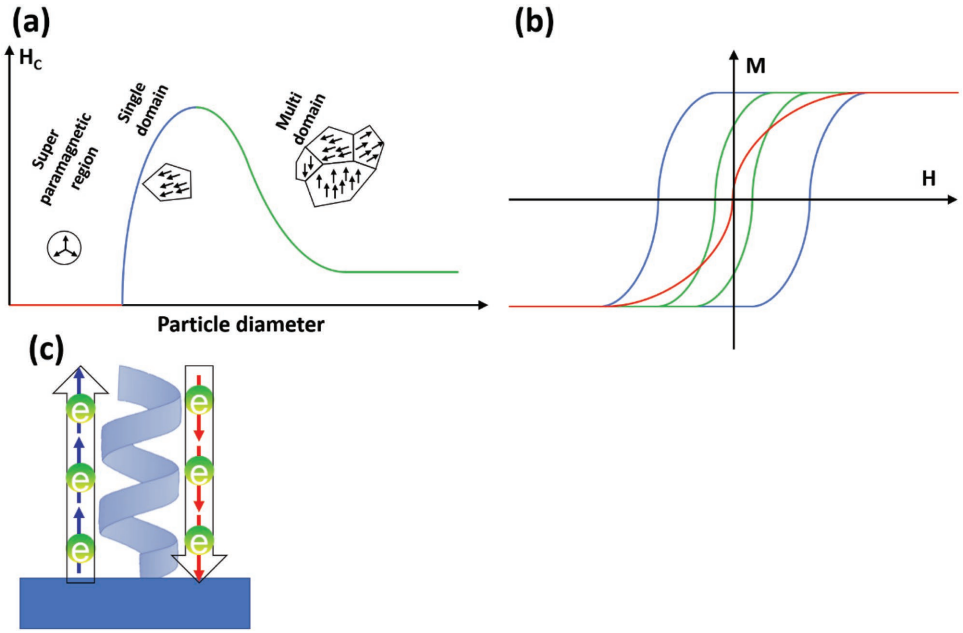

Figure 1. Panel (a) shows the generic dependence of a magnetic material (FM in the bulk) on the reduction physical size: multidomain (green), single domain (blue), and superparamagnetism (red). Panel (b) shows magnetization hysteresis loops for the different domain size behaviors. Panel (c) illustrates the CISS effect in which a right-handed chiral molecule has preference for spin up to move upward and for spin down to move downward.

and experimentally determined to be 76 nm[7] and for spherical Fe_3O_4 nanoparticles the theoretical critical diameter was found to be 128 nm.[8] Reducing the size of the material even further destabilizes the magnetization and its magnetic orientation becomes susceptible to thermal fluctuations and weak stray magnetic fields. At small enough sizes, the material enters the superparamagnetic regime, ≈10–20 nm scale, with zero coercivity and no magnetic remanence (**Figure 1**a,b).[9] Thus, the reduction in size of magnetic memory devices and magnetic reading heads is usually limited to a 30–50 nm size regime.[10]

In recent works, it was shown that simple spintronic devices without magnetic layers could be realized using the chiral-induced spin selectivity (CISS) effect.[11,12] The CISS effect provides an easy and efficient way to generate a spin polarized current that is either parallel or antiparallel to the electrons' velocity. In addition, it correlates with the handedness of the chiral molecules. Using the CISS effect, new types of simple spintronic memory devices and a nanoscale memristor have been demonstrated.[13–16]

The adsorption of chiral molecules on a metal surface has been shown to change the metal's magnetic properties[17–20] and also switch the magnetization direction of a soft FM in a way that depends on the handedness of the chiral molecules.[21] This effect was named the magnetism induced by proximity of adsorbed chiral molecules, and it arises from the CISS effect, i.e., the spin-dependent electron fluctuations in chiral molecules. For right-handed (left-handed) chiral molecules electrons with a preferred spin up (down) move upward through the molecule and electrons with a preferred spin down (up) move downward through the molecule (Figure 1c). In a semiclassical picture, placing chiral molecules with these charge oscillations in contact with a metal induces a magnetic moment in the metal by spin torque transfer.[22–24] In a more quantum picture, the proximity induced wavefunction delocalization of surface states occurs upon surface modification,[25,26] and the wavefunction penetration into the chiral molecules is spin dependent because of the CISS effect. This phenomenon induces a nonsymmetric density of states in the material, which is equivalent to magnetization of a ferromagnetic. Note that these works show that chiral molecules can reorder magnetization or induce paramagnetism. However, no reports have claimed that superparamagnetism can be changed to ferromagnetism.

In the present work, we show that chiral molecules can change the magnetic properties of 10 nm iron oxide nanoparticles from superparamagnetic to ferromagnetic, thus realizing 10 nm chiral induced ferromagnetic iron oxide nanoparticles (CIFIONs). These CIFIONs present ferromagnetic properties even at 10 nm size. The anisotropic placement of the chiral molecules stabilizes the nanoparticles magnetization direction at room temperature and the orientation depends on the handedness of the chiral molecules. These studies point to a novel method for the miniaturization of well-defined ferromagnets (≈10 nm) using established synthetic protocols for superparamagnetic iron oxide nanoparticles (SPIONs).

In this work, we used ≈10 nm spherical SPIONs capped by oleic acid, oleylamine, and 1,2 dodecanediol in a chloroform solution, which were synthesized following a previously reported procedure.[27,28] **Figure 2**a shows a representative transmission electron microscopy image of the as-synthesized SPIONs. As a reference system, we also used SPIONs capped by L- tartaric acid molecules in a water solution (Figure S1, Supporting Information).

Right-handed (L) and left-handed (D) α-helix polyalanine (AHPA) were used as the chiral molecules to imprint a magnetization on the iron oxide nanoparticles. The chiral molecules were purchased from Sigma-Aldrich Co. LLC, with a sequence

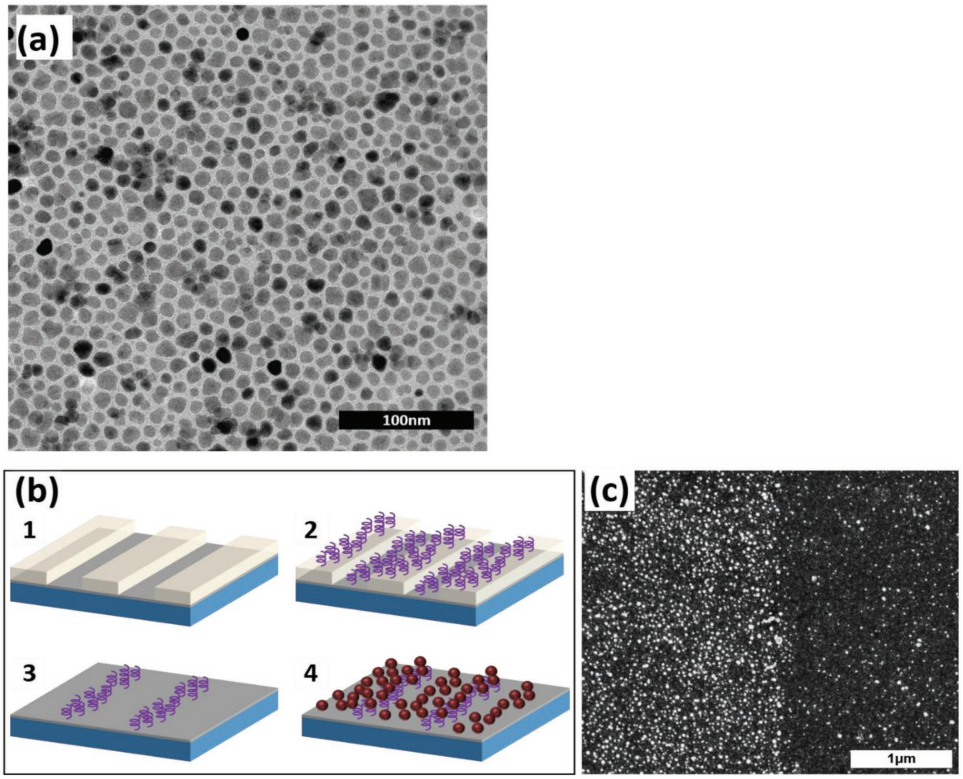

Figure 2. a) Transmission electron microscope image of the ≈10 nm SPIONs. b) Illustration of the M-AFM samples patterning of the AHPA-SAM on a 100 nm Ag (gray layer) evaporated on 4 × 4 mm^2 Si chip (blue layer). 1-the resist pattern. 2-AHPA-SAM (purple helical molecules) formation. 3-Resist lift-off, AHPA-SAM was left only where there was no resist. 4-iron oxide nanoparticle (red spheres) adsorption. c) Scanning electron microscope image on the border between an area with AHPA-SAM (left side) and an area without (right side). The iron oxide density is much higher on the AHPA-SAM because of the carboxylic terminal group of the AHPA molecule which binds to iron oxide.

of 36 amino acids of [H]-CAAAAKAAAAKAAAAKAAAAKAAA AKAAAAKAAAAK-[OH] where C, A, and K are cysteine, alanine, and lysine amino acids, respectively. The AHPA molecules are terminated with a thiol group from the cysteine amino acid and a carboxylic terminal group through the last lysine residue. The thiol is used to covalently bind the AHPA molecules to metal surfaces such as gold and silver and the carboxylic group was used to bind and immobilize the SPIONs.

Measurement of the magnetization imprinting effect on the SPIONs by the AHPA molecules was performed with a superconducting quantum interference device (SQUID) and by using magnetic atomic force microscopy (M-AFM). For both types of measurements, the sample consisted of a monolayer film of SPIONs supported by a self-assembled monolayer (SAM) of L- or D- AHPA, on a 100 nm Ag film. For the M-AFM measurement, additional lithography was performed to pattern AHPA-SAM areas with lift-off assisted selective adsorption (Figure 2b outlines this procedure) in order to compare SPIONs with and without chiral molecules in the same M-AFM image. M-AFM measurements were obtained by taking interleaved topography and magnetic interaction images using a cobalt alloy-coated tip (coercive field of ≈300 Oe, K ~ 2.8 N m^{-1}, F ~ 75 KHz) which was magnetized either normal (up) or antinormal (down) to the substrate with a 5000 Oe magnetic field. Scanning electron microscopy images taken at the border between an AHPA-SAM (left side) and bare silver (right side) show that a higher particle density is present on the AHPA-SAM areas (Figure 2c). The higher SPION density is attributed to the carboxylic terminal group of the AHPA molecule.

For the M-AFM measurements, two additional reference samples were prepared. The first reference sample had only SPIONs on Ag (without AHPA). The second reference sample used SPIONs that were coated from all directions with L-tartrate (or D-tartrate) ligands and placed on a mica substrate, to check the importance of symmetry breaking.

Preparation and measurements details of all samples are available in the Supporting Information.

Magnetic moment measurements of SPIONs adsorbed on L-AHPA molecules (**Figure 3**a) were performed using a SQUID, and the magnetization hysteresis loop was obtained (Figure 3b) by subtracting the response of a clean Ag substrate (see Figure S3 in the Supporting Information).[29] The SPIONs by themselves do not show significant magnetization when deposited on an Ag substrate (blue). The adsorption of chiral molecules on the Ag substrate generates a weak additional magnetism (green), which may arise from chiral imprinting.[21] Interestingly, when the SPIONs are deposited on the L-AHPA-SAM the hysteresis loop inverts and a stronger magnetization is recorded (purple). Despite the intrinsic property of SPIONs to be superparamagnetic, i.e., zero coercivity and no remanence field, upon their adsorption on chiral molecules the SPIONs transform into CIFIONs with a ferromagnetic hysteresis loop

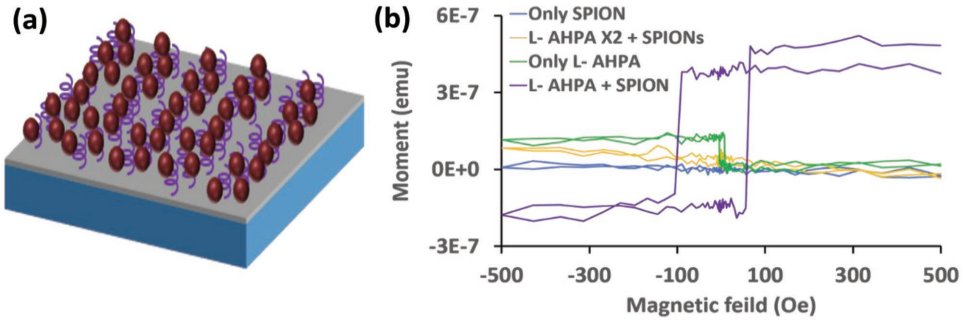

Figure 3. a) Illustration of the sample for the SQUID measurements: 100 nm Ag (gray layer) evaporated on 4 × 4 mm^2 Si chip (blue layer). SAM of AHPA chiral molecules (purple helical molecules) was adsorbed on the Ag layer and iron oxide nanoparticles (red spheres) were adsorbed on top of the AHPA-SAM. b) SQUID measurements of the magnetization hysteresis loop. The sample of L-AHPA with iron oxide nanoparticles (purple line) shows CIFIONs with a hysteresis loop exhibiting ferromagnetic behavior with an average coercive field of ≈80 Oe. The hysteresis loop is not symmetric around zero and shows a preference to magnetize the CIFIONs in the upward direction. Three reference samples were measured. The first of L-AHPA X2 with chiral molecules adsorbed on both sides of the iron oxide nanoparticles (orange line) display no measurable response. The second of only L-AHPA (without nanoparticles, green line) shows weak magnetic order and no hysteresis is measured. In this case, the adsorption of chiral molecules from one side also seem to generate some small substrate magnetic ordering. The third reference sample of only iron oxide nanoparticles (without AHPA, blue line) presents no measurable response.

and average coercive field of ≈80 Oe. The hysteresis loop is not symmetric around zero and shows a preference to magnetize the CIFIONs in the upward direction. All measurements were repeated on three samples.

To relate this effect to the adsorption of chiral molecules from one side only, a reference sample with an additional L-AHPA-SAM adsorbed on top of the SPIONs, named L- AHPA X2 (the SPIONs are now embedded between two layers of L-AHPA molecules), was prepared. Figure S2 in the Supporting Information illustrates the preparation. In this case, no significant magnetization was measured (orange); it was similar to the measurement with only SPIONs deposited on silver. The hysteresis loop is not symmetric around zero and shows a preference to magnetize the CIFIONs in the upward direction. The flip from upward to downward magnetization occurs at ≈–95 Oe, whereas the flip from downward to upward magnetization occurs at ≈60 Oe. In all of the reference samples (without the SPIONs), the hysteresis was below the noise level. It is interesting to note that the magnetic moment seems to be symmetric around the L-AHPA curve. It is clear that the chiral molecules impart some magnetization onto the substrate, which may give rise to the asymmetry around zero magnetic field.

Figure 4 shows the results of the M-AFM measurements. For the L-AHPA (right-handed helix), the SAM was patterned into stripes (topography images are shown in Figure 4a,b and magnetic interaction images are shown in Figure 4d,e for downward and upward magnetization of the M-AFM tip, respectively). When magnetizing the M-AFM tip downward (red arrow), a repulsive magnetic interaction is measured (bright features), and for an upward magnetized tip (blue arrow), an attractive magnetic interaction is observed (dark features). This behavior demonstrates that the CIFIONs are magnetized with an upward orientation. For D-AHPA (left-handed helices), the SAM was patterned into squares; the topography image is shown in Figure 4c and the magnetic interaction image for downward magnetization of the M-AFM tip is shown in Figure 4f. In this case, an attractive interaction dominates which indicates that the CIFIONs are magnetized with a downward orientation. This observation stands in contrast to Figure 4d in which L-APHA CIFION samples, probed with the same tip magnetization, show the opposite behavior. Thus, the chirality of the AHPA SAM controls the orientation of the magnetization the iron oxide nanoparticles. Similar measurements are presented for an individual nanoparticle in Figure S4 in the Supporting Information.

Two additional reference systems were investigated using M-AFM. The first reference measured the magnetic interaction of SPIONs physically adsorbed on an Ag layer without any chiral molecules (**Figure 5**a–c and see Figure S5 in the Supporting Information for topography cross-section images). These data fail to generate a discernable magnetic response above the background. In the second system, SPIONs were covered on all sides with L-tartaric acid and were measured by the M-AFM method on a mica surface (Figure 5d–f). These nanoparticles displayed a random magnetization direction. Additional images for L- and D-tartaric acid SPIONs on SiO_2 and statistical analysis thereof are shown in Figure S6 in the Supporting Information.

The experimental results indicate that the chiral molecules change the magnetic properties of SPIONs from superparamagnetic, which has zero coercive field and no remanence, to ferromagnetic CIFIONs, which have a nonzero coercive field and display remanence. The SQUID measurements exhibit a significant ferromagnetic hysteresis loop for CIFIONs on an AHPA-SAM with an average coercive field of ≈80 Oe, while the reference measurements of only SPIONs or only AHPA-SAMs show no hysteresis loops and much weaker magnetic signals (Figure 3b). The hysteresis loop is also not symmetric around zero magnetic field, which indicates that magnetization of the CIFIONs in the upward direction requires a lower absolute magnetic field than in the downward direction for the right-handed helical molecules (L-AHPA).

The M-AFM measurements show that the CIFIONs on an L-AHPA SAM have attractive or repulsive magnetic interactions with the M-AFM tip when the tip is magnetized in the

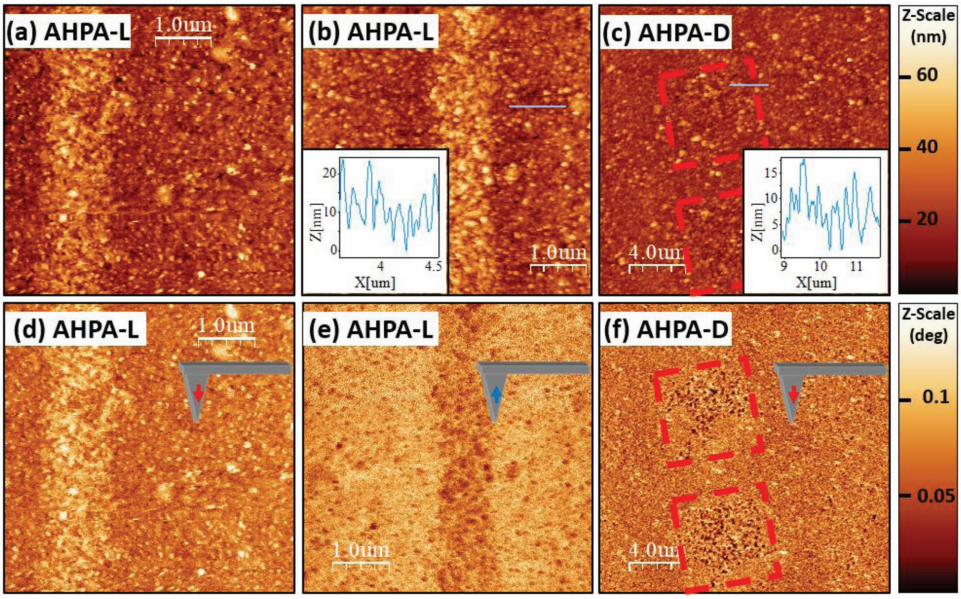

Figure 4. Panels (a–c) show topography images that were taken and interleaved with the magnetic interaction images (tip distance of 130 nm) in panels (d–f). Topography and phase color scales are on the respective right sides of the images. The M-AFM tip was magnetized down (red arrow), or up (blue arrows). In panels (d) and (e) an L-AHPA-SAM (right-handed), the substrate, is patterned with lines and shows that the iron oxide nanoparticles are magnetized upward. The tip experiences repulsive interactions for downward tip magnetization and attractive interactions for upward tip magnetization, as indicated by the bright and dark colors. In panel (f), D-AHPA-SAM (left handed) has a square patterned surface (red squares) and the darker color shows that the iron oxide nanoparticles are magnetized downward due to attractive magnetic interactions with a downward magnetized M-AFM tip. The insets in panels (b) and (c) show topographic cross sections.

down and up orientations, respectively. This dependence is reversed for CIFIONs on a D-AHPA SAM (Figure 4f). These results corroborate the SQUID measurements by showing that the functionalized iron oxide nanoparticles exhibit a stable magnetization, which is robust to thermal fluctuations and displays a significant coercive field and remanence (in contrast to a nanoparticle with superparamagnetic behavior). The measurements also show that the orientation of the CIFION magnetization is controlled by the chirality of the SAM molecules.

We ascribe the chiral-based magnetization imprinting on the SPIONs to chiral-induced spin selectivity at the chiral molecule–iron oxide interface. An electron exchange current flows

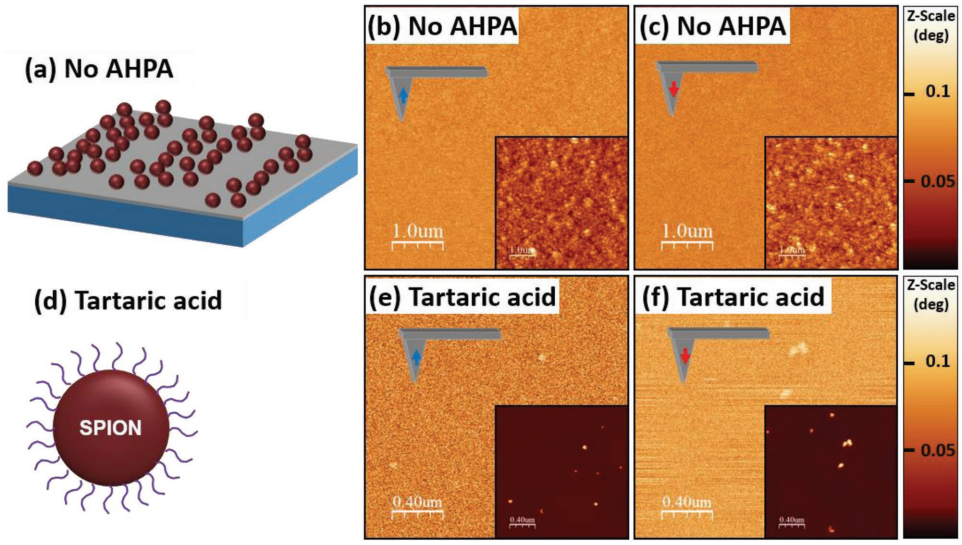

Figure 5. a) Illustration of the SPIONs with no chiral molecule reference sample. b,c) Magnetic interaction measurements of SPIONs on Ag without chiral molecules. There is no measurable signal for both M-AFM tip magnetizations (upward and downward) although there are SPIONs as can be seen in the topography images (insets). d) Illustration of SPION covered, from all directions, with left-handed chirality tartaric acid. e,f) Magnetic interaction measurements of tartaric acid covered SPIONs on a mica substrate. For both tip magnetization (upward and downward), there is a repulsive magnetic interaction, which correlates to the SPIONs seen in the topography images (insets).

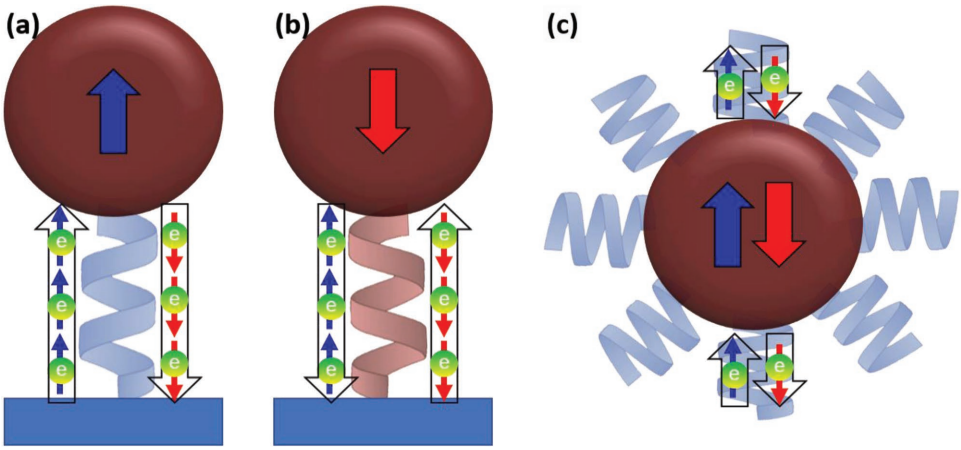

Figure 6. Panels (a) and (b) show right-handed and left-handed chiral molecules, respectively, linked only to the bottom side of the iron oxide nanoparticle. Because of the CISS effect, spin up (down) electrons are preferentially going into the nanoparticle, while spin down (up) electrons are preferentially going out of the nanoparticle creating majority spin up (down) electrons in the nanoparticle. This process creates a net magnetization of the nanoparticle with a defined upward (downward) orientation. Panel (c) shows a right-handed chiral molecule linked to the iron oxide nanoparticle from all directions. In this case, spin up (down) electrons are going into the nanoparticle from the bottom (top) chiral molecule and going out of the nanoparticle from the top (bottom) molecule, resulting in unstable magnetization.

between the iron oxide nanoparticles and the Ag substrate by way of the chiral molecules, and the forward and reverse current are spin filtered by the chiral molecules. The spin preference is determined by the helicity of the chiral molecule; for right-handed (left-handed) chiral molecules spin up (down) electrons will be preferentially transmitted to the molecule, while spin down (up) electrons will be preferentially transferred down the molecule. This process results in a majority spin up population in the nanoparticle and stabilizes the magnetization in the upward direction (**Figure 6**a). The opposite magnetization of the iron oxide nanoparticle is observed when the chirality of helical molecules is reversed (Figure 6b). In the case of a SPION covered by chiral molecules from all directions or embedded between two SAMs of the same handedness, the symmetry plane is not broken and no net stable magnetization is observed; an electron with one type of spin will transfer into the SPION from the bottom interface with chiral molecules, while the interface at the top of the SPION will transfer electrons of the opposite spin type (Figure 6c).

Measurements (both SQUID and M-AFM) of the reference samples of SPIONs without chiral molecules do not show magnetization and substantiate the role of chiral-induced spin selective transport for the magnetization imprinting. The magnetic interaction measurements on chiral tartaric acid coated SPIONs indicate that achieving strong magnetization imprinting requires anisotropic coverage, e.g., a defined orientation for spin flow.

Using SQUID and M-AFM measurements, we have shown how ferromagnetic properties can be imprinted on 10 nm SPIONs. This size reduction should enable the scale down of magnetic memory area by an order of magnitude and may prove to be important to magnetic force microscopy as well. These magnetic chiral iron oxide nanoparticles manifest remanence and an average coercive field of ≈80 Oe at room temperature. In addition, the preferred magnetization direction is determined by the chirality of the molecules and their nonsymmetrical placement around the nanoparticle. We propose a mechanism for the chiral imprinting that is based on the well-established CISS effect; namely, magnetism induced by proximity of adsorbed chiral molecules. This explanation suggests that the ferromagnetic properties are imprinted when the chiral molecules are bound on one side of the SPIONs and should disappear when the SPIONs are covered with chiral molecules from two opposite faces, or from all directions. Measurements of SPIONs covered with chiral molecules from two or all directions indeed showed no remanence and zero coercive field. The results indicate that magnetic-based devices (especially spintronic devices) can be further miniaturized using chiral-based magnetization imprinting and that magnetic nanomaterials could be magnetized using chemical adsorption, without an external magnetic field and without applying spin-polarized current.

Supporting Information

Supporting Information is available from the Wiley Online Library or from the author.

Acknowledgements

Y.P. acknowledges the support from the Volkswagen Foundation (No. VW 88 367), the Israel Science Foundation (ISF Grant No. 1248/10), and the MOS Israel. R.N. acknowledges support in part from the European Research Council under the European Union's Seventh Framework Program (No. FP7/2007-2013)/ERC Grant Agreement No. (338720), the MOS Israel, and the VW Foundation (No. VW 88 367). D.P. acknowledges the Israel Science Foundation (ISF grant 1589/14) and the Minerva Centre for biohybrid complex systems. D.P. also thanks the Etta and Paul Schankerman Chair of Molecular Biomedicine. D.H.W. and R.N. acknowledge support by the U.S. Department of Energy; Grant No. ER46430.

Conflict of Interest

The authors declare no conflict of interest.

[1] M. Guth, G. Schmerber, A. Dinia, *Mater. Sci. Eng., C* **2002**, *19*, 129.
[2] S. Bhatti, R. Sbiaa, A. Hirohata, H. Ohno, S. Fukami, S. N. Piramanayagam, *Mater. Today* **2017**, *20*, 530.
[3] C. S. Hwang, *Adv. Electron. Mater.* **2015**, *1*, 1400056.
[4] Y. Huai, **n.d**., *8*.
[5] T. Kawahara, K. Ito, R. Takemura, H. Ohno, *Microelectron. Reliab.* **2012**, *52*, 613.
[6] "Ferromagnetism." Available at http://hyperphysics.phy-astr.gsu.edu/hbase/Solids/ferro.html.
[7] Q. Li, C. W. Kartikowati, S. Horie, T. Ogi, T. Iwaki, K. Okuyama, *Sci. Rep.* **2017**, *7*, 9894.
[8] D. L. Leslie-Pelecky, R. D. Rieke, *Chem. Mater.* **1996**, *8*, 1770.
[9] A. S. Teja, P.-Y. Koh, *Prog. Cryst. Growth Charact. Mater.* **2009**, *55*, 22.
[10] A. Hirohata, K. Takanashi, *J. Phys. D: Appl. Phys.* **2014**, *47*, 193001.
[11] R. Naaman, D. H. Waldeck, *J. Phys. Chem. Lett.* **2012**, *3*, 2178.
[12] R. Naaman, D. H. Waldeck, *Annu. Rev. Phys. Chem.* **2015**, *66*, 263.
[13] O. B. Dor, S. Yochelis, S. P. Mathew, R. Naaman, Y. Paltiel, *Nat. Commun.* **2013**, *4*, 2256.
[14] O. Ben Dor, N. Morali, S. Yochelis, L. T. Baczewski, Y. Paltiel, *Nano Lett.* **2014**, *14*, 6042.
[15] G. Koplovitz, D. Primc, O. Ben Dor, S. Yochelis, D. Rotem, D. Porath, Y. Paltiel, *Adv. Mater.* **2017**, *29*, 1606748.
[16] H. Al-Bustami, G. Koplovitz, D. Primc, S. Yochelis, E. Capua, D. Porath, R. Naaman, Y. Paltiel, *Small* **2018**, *14*, 1801249.
[17] I. Carmeli, G. Leitus, R. Naaman, S. Reich, Z. Vager, *J. Chem. Phys.* **2003**, *118*, 10372.
[18] P. Crespo, R. Litrán, T. C. Rojas, M. Multigner, J. M. de la Fuente, J. C. Sánchez-López, M. A. García, A. Hernando, S. Penadés, A. Fernández, *Phys. Rev. Lett.* **2004**, *93*, 087204.
[19] A. Hernando, P. Crespo, M. A. García, *Phys. Rev. Lett.* **2006**, *96*, 057206.
[20] Y. Yamamoto, T. Miura, M. Suzuki, N. Kawamura, H. Miyagawa, T. Nakamura, K. Kobayashi, T. Teranishi, H. Hori, *Phys. Rev. Lett.* **2004**, *93*, 116801.
[21] O. B. Dor, S. Yochelis, A. Radko, K. Vankayala, E. Capua, A. Capua, S.-H. Yang, L. T. Baczewski, S. S. P. Parkin, R. Naaman, Y. Paltiel, *Nat. Commun.* **2017**, *8*, 14567.
[22] L. Berger, *Phys. Rev. B* **1996**, *54*, 9353.
[23] J. C. Slonczewski, *J. Magn. Magn. Mater.* **1996**, *159*, L1.
[24] D. C. Ralph, M. D. Stiles, *J. Magn. Magn. Mater.* **2008**, *320*, 1190.
[25] M. Kisielewski, A. Maziewski, M. Tekielak, A. Wawro, L. T. Baczewski, *Phys. Rev. Lett.* **2002**, *89*, 087203.
[26] M. Kisielewski, A. Maziewski, Z. Kurant, M. Tekielak, A. Wawro, L. T. Baczewski, *J. Appl. Phys.* **2003**, *93*, 7628.
[27] N. Depalo, P. Carrieri, R. Comparelli, M. Striccoli, A. Agostiano, L. Bertinetti, C. Innocenti, C. Sangregorio, M. L. Curri, *Langmuir* **2011**, *27*, 6962.
[28] N. Depalo, R. M. Iacobazzi, G. Valente, I. Arduino, S. Villa, F. Canepa, V. Laquintana, E. Fanizza, M. Striccoli, A. Cutrignelli, A. Lopedota, L. Porcelli, A. Azzariti, M. Franco, M. L. Curri, N. Denora, *Nano Res.* **2017**, *10*, 2431.
[29] Chemical Rubber Company, in *CRC Handbook of Chemistry and Physics*, CRC Press, Cleveland, Ohio **1978**, pp. 4–142.